Journal of Engineering and Applied Sciences 13 (13): 5150-5161, 2018
ISSN: 1816-949X

Investigation of Effective Hybrid FRP and Steel Reinforcement Ratio for Concrete Members

Hayder H. Alkhudery, Oday M. Albuthbahak and Haider A.A. Al-Katib
Faculty of Engineering, Kufa University, Najaf, Iraq

Abstract: Fiber Reinforced Material (FPR) has become an effective alternative reinforcement for concrete constructions owing to their higher ultimate strength in tension and strongly anticorrosive properties. However, the low ductility behaviour of FRP Reinforcing Concrete structure (FRP-RC) is appeared comparing to high ductility of conventional Steel Reinforcing Concrete structures (S-RC). Successfully hybridization of reinforcement by combining FRP and steel rebar presents effective solution to migrate corrosion of steel rebar in steel reinforcing concrete constructions and advanced ductility of FRP-RC structures. Also, a good improvement is achieved in structural performances of concrete beams in terms of ultimate strength, central deflection, number cracks and crack width. In this study, a theoretical prediction analysis model of Hybrid Reinforcing Concrete (H-RC) members reinforced by FRP and steel rebar presents. The moment-curvature relationship is predicted to achieve load-deflection curve and bending moment capacity of beams. A good agreement has been indicated from verification between results of predicted theoretical model and 19 experimental results of other researcher. The hybrid reinforcement in HRC section can be replaced by equivalent steel ratio to conduct limitations of reinforcement ratio. The ductility index of H-RC members is measured to reference S-RC member while the ultimate strength index is measured to reference FPRC member. A critical limitations of (A_f/A_s) ratio is found for H-RC members for specified mechanical properties of concrete, steel and FRP rebar also, this limitations are affected by the equivalent steel ratio of hybrid concrete section. A parametric study of different parameters specially that influencing the amount of hybridization reinforcing ratio (A_f/A_s) is involved to explore the critical margin of (A_f/A_s) ratio utilizing the ductility and ultimate strength requirements. Also, various modes of failure were conducted to the corresponding area of reinforcing FRP and steel rebar.

Key words: Theoretical prediction model, FRP and steel reinforcements, hybrid reinforced concrete members, flexural investigation, ductility index, ultimate strength

INTRODUCTION

In the last decades Fiber Reinforcing Polymers (FRPs) are using as reinforcing materials for the concrete constructions because of their higher corrosion resistance and a high ratio of strengthen to weight. Moreover, they are nonconductive to electrical power and nonmagnetic, making them attractive as alternatives to traditional steel reinforcing rebar in concrete structures with severe environments or special situations such as transparency is required. Besides all these advantages, FRP rebar have mainly two disadvantages which are brittleness and low elasticity modulus. For pure FRP-Reinforcing Concrete (FRP-RC) beams, elastic behaviour of FRP rebar is linearly upward to failure (i.e., without yield point) which is caused brittle failure mode without warning rather than ductile. Codes of design adopted over reinforcing FRP principle for designing criterion which is further gradual and reduced probability to sudden collapse with more deformability grade. Furthermore, ductility lack for FRP rebar due to low of elasticity constant comparing with steel rebar, consequently, FRP-RC members suffer large deflection and widening crack width than Steel Reinforcing Concrete (S-RC) members having the same cross section and reinforcing ratio. However, designing criterion of FRP-RC structures based on service ability limit states which ensure structural behaviour instead of the strength to verify safety and functional of the structures within expect life. Structural performances of concrete structures are enhanced by merging FRP and steel reinforcements (hybrid reinforcements) in order to migrate corrosion problem caused by Steel Rebar in SRC structures and advanced ductility of FRP-RC structures. Hybrid reinforcements (FRP and steel rebar) present a realistic and appropriate solution for structural concrete design. Tan (1997) investigate hybrid reinforced concrete members were reinforced by Aramid-Fiber Reinforcing Polymer (AFRP) and steel rebar. He indicated that sufficient serviceability parameters have been utilized when the amount of AFRP reinforcement area less than one half of the whole reinforcement (Tan, 1997). Aiello and Ombres (2002) concluded by placing steel rebar on interior level and FRP rebar close to exterior face of tension region, the stiffness of hybrid reinforcing

Corresponding Author: Hayder H. Alkhudery, Faculty of Engineering, Kufa University, Najaf, Iraq

members is increased. Thus, the steel reinforcement within hybridization section have less involvement to the ultimate strength, whilst it provides an effective contribution regarding ductile and structural stiffness performance also, the crack widening and spacing is diminished (Aiello and Ombres, 2000). Leung and Balendran (2003) were explored the flexure behaviour of H-RC members reinforced by GFRP and steel rebar which located at different effective depth. They indicated that at stage of loading after yielding of steel rebar is occurred, the ultimate strength of H-RC member is increased as the FRP reinforcement strength is increased (Leung and Balendran, 2003). Qu *et al.* (2009), carried out experimental program for H-RC members with hybrid reinforcing steel and (GFRP) rebar, they indicated by presenting a sufficient amount of steel to GFRP reinforcement, the beam's ductile and serviceability can be enhanced. Lau and Pam (2010) were reported the hybridization of reinforcement strongly improved the ductility of H-RC members in comparison with FRP-RC members throughout experimental program as well. Hawileh (2015) studied H-RC beams using numerical approach represented by FEA model with AFRP and steel reinforcements, he found that the compressive strength of concrete has moderate effected on flexural behaviour features (Hawileh, 2015). Ilker *et al.* presented a numerical model for H-RC section. They found that the FRP reinforcement a core of loading resistance after steel is yielding (Kara *et al.*, 2015).

Previous research programs were concentrated mainly on the strength evaluation, failure models, load-deflection response and cracking patterns in H-RC beams. These beams were reinforcing by various FRP rebar types and containing a large range of reinforcing ratio with dissimilar in geometry and mechanical parameters. The obtaining tested results ensured the efficiency of steel rebar to improve the structural behaviour of H-RC beams in terms of ductility index and serviceability limitations comparing with FRP-RC members. However, the ductility issue remains focal of structural capability aspects of H-RC members, yet, needed more investigation. It stills unrecognized the conditions to be introduced H-RC members having ductility features similar to that of S-RC members. Extra investigation of experimental and theoretical programs should be provided to clarify reinforcement hybridization features.

In this study, a theoretical model has been introduced to study the flexure behaviour of H-RC concrete members. This model based on forces equilibrium and compatibility of strain to establish the moment-curvature relations (M-Ø), the load-deflection and flexural capability of H-RC beams. A good agreement has been indicated from verification between results of predicted theoretical model and 19 experimental results of other researcher. The hybrid reinforcement in H-RC section can be replaced by equivalent steel ratio to conduct limitations of reinforcement ratio. The ductility index of H-RC members is measured to reference S-RC member while the ultimate strength index is measured to reference FPR-RC member. A critical limitations of A_f/A_s ratio is found for H-RC members with specified mechanical properties of concrete, steel and FRP rebar and this limitations are affected by the equivalent steel ratio of hybrid concrete section. Also, a parametric study of different parameters specially that influencing the amount of hybrid reinforcing ratio (A_f/A_s) is involved to explore the critical margin of A_f/A_s ratio utilizing the ductility and ultimate strength requirements. Also, various modes of failure were conducted to the corresponding area of reinforcing FRP and steel rebar.

MATERIALS AND METHODS

Theoretical model: A theoretical model is introduced to formulate a flexure response of FRP/steel reinforced concrete (i.e., H-RC) beam. Using equilibrium of forces and compatibility of strains, the moment curvature relation is established of H-RC member. Then mid-span deflection of the beam determined using relative curvature of mid-span. The adopted approach illustrated in more details as follows.

Stress-strain relationships of materials: In this investigation, the stress strain relations of implemented materials concrete and reinforcing steel and FRP rebar are presented in Fig. 1. Other material models can be adopted in proposed model. The adopted model of stress strain relation for concrete under compressive loading that proposed by Hognestad *et al.* as descried in Eq. 1 and Fig. 1a (Qu *et al.*, 2009):

$$f_c(\varepsilon_c) = f_c'\left(\frac{2\varepsilon_c}{\varepsilon_{co}} - \left(\frac{\varepsilon_c}{\varepsilon_{co}}\right)^2\right) \text{ if } \varepsilon_c \le \varepsilon_{co} \quad (1)$$

$$f_c(\varepsilon_c) = f_c'\left(1 - 0.15\,\frac{(\varepsilon_c - \varepsilon_{co})}{(\varepsilon_{cu} - \varepsilon_{co})}\right) \text{ if } \varepsilon_{co} \le \varepsilon_c \le \varepsilon_{cu} \quad (2)$$

Where:

f_c' = Cylinder concrete compressive strength
ϵ_c = Concrete compressive strain
ϵ_{co} (= 1.8 f_c'/E_c) = Concrete strain with peak stress
ϵ_{cu} = 0.0038 = Ultimate concrete compressive strain
E_c (= 4700↓ f_c') = Concrete elasticity constant (ACI, 318-05, 2005)

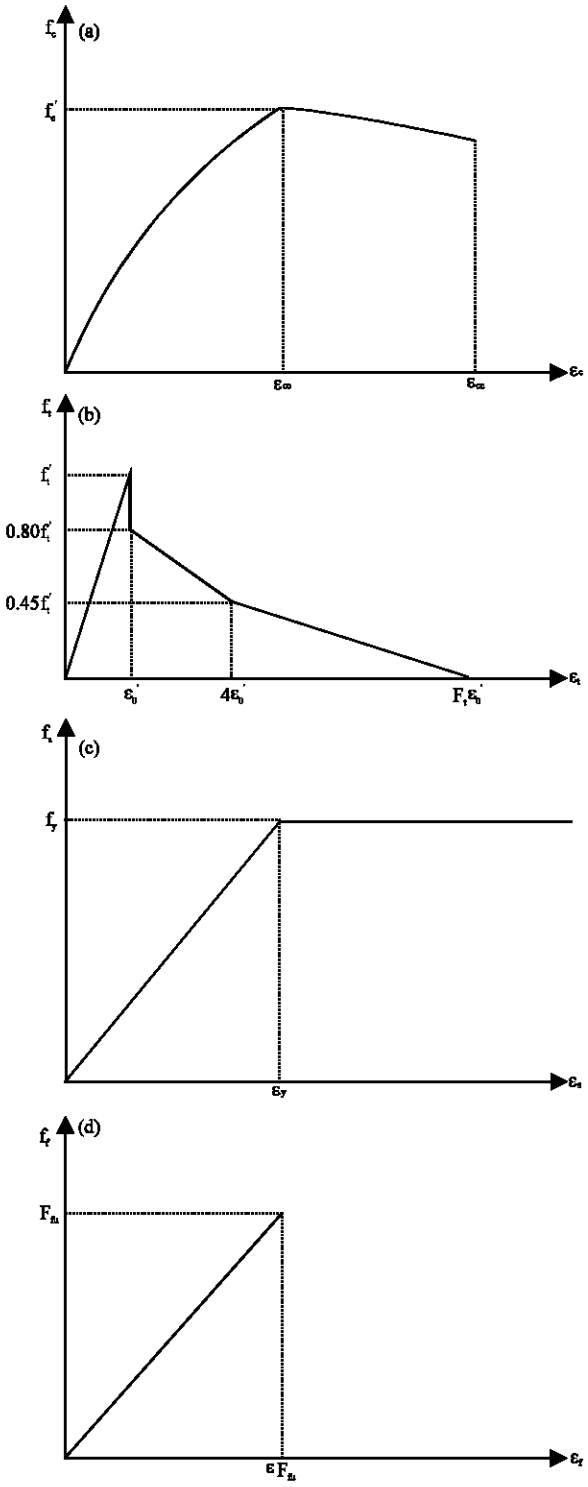

Fig. 1: Concrete, steel and FRP reinforcement stress strain relations (Qu *et al*., 2009; Bischoff and Paixao, 2004; Nayal and Rasheed, 2006): a) Concrete in compression; b) Concrete in tension; c) Steel-reinforcement and d) FRP-reinforcement

Bischoff and Paixao (2004) determined the tensile strength for H-RC members, they concluded that the less concrete tensile strength is exhibited by S-RC beam in comparison with GFRP-RC members. Nayal and Rasheed (2006) investigated the behavior of S-and FRP-RC members in terms of tensile strength effects, they used a reverse integration technique of non-linear numeric evaluation and experiment results to provide a concrete tensile strength model for concrete member with hybrid reinforcements as described in Eq. 2 and shown in Fig. 1b:

$$f_t = E_c\,\varepsilon_t \quad \text{if } 0 \le \varepsilon_t \le \varepsilon_0' \tag{3}$$

$$f_t = 0.45\,f_t' + 0.35\,f_t'\left(\frac{4\varepsilon_0' - \varepsilon_t}{3\varepsilon_0'}\right) \text{if } \varepsilon_0' \le \varepsilon_t \le 4\varepsilon_0' \tag{4}$$

$$f_t = 0.45\,f_t' + 0.35\,f_t'\left(\frac{F_t\varepsilon_0' - \varepsilon_t}{F_t\varepsilon_0' - 4\varepsilon_0'}\right) \text{if } 4\varepsilon_0' \le \varepsilon_t \le F_t 4\varepsilon_0' \tag{5}$$

$$F_t = 124 - 0.05\,\lambda \tag{6}$$

$$\lambda = \frac{E_s\,A_s + E_f\,A_f}{n_s'\,d_s + n_f'\,d_f} \tag{7}$$

Where:

f_t = Concrete tension stress
ϵ_t = Concrete tension strain
$\epsilon_0' = f_t'/E_c$, f_t' (= 0.26 3↓ $f_c'^2 u$) = Concrete tension strength
F_t = Proportional factor of the maximum strain in tension to the strain of concrete cracking
E_s = Elasticity constant of steel rebar
A_s = Steel area
E_f = Elasticity constant of FRP rebar
A_f = FRP area
n_s = Steel rebar number
d_s = Steel rebar diameter
n_s' = FRP rebar number
d_f = Rebar FRP diameter
λ = kN/mm
F_t = kN/mm

The multilinear descending mode of concrete in tension reflects initially and secondary cracking of concrete. Researchers were suggested special values, $F_t = 100$ to the FRP rebar and $F_t = 10$ to the steel rebar. Since, the parameter F_t designate the variance of S-and FRP-RC members in tensile strength. Also, factor λ, collected the sectional geometry parameters which showing the tensile strength behaviour and that is

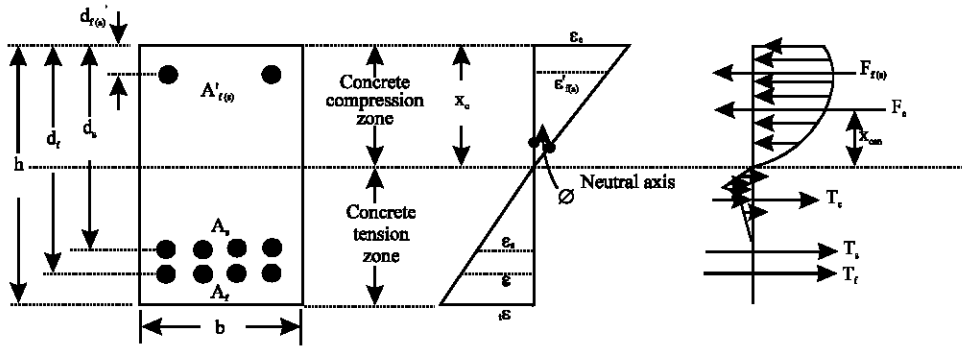

Fig. 2: Hybrid FRP and steel reinforcing concrete section stress, strain distribution and forces: a) Hybrid reinforcing concrete section; b) Strain division and c) Stress division and forces

explained the variance of F_t magnitudes for steel in comparison with FRP reinforcing rebar (Bischoff and Paixao, 2004). A bi-linear elastic perfect plastic is the adopted material model of reinforcing steel with yield stress f_y as shown in Fig. 1c and given in Eq. 8 and 9:

$$f_s = E_s\varepsilon_s \quad \text{if } 0 \le \varepsilon_s \le \varepsilon_y \tag{8}$$

$$f_s = f_y \quad \text{if } \varepsilon_s > \varepsilon_y \tag{9}$$

Where:
f_s = Steel tension stress
E_s = Steel elasticity constant
ϵ_s = Steel tension strain
ϵ_y = Steel yielding tension strain

And linear elastic up to rupture, the stress strain relationship of FRP rebar as presented in Fig. 1d and described by Eq. 10 and 11:

$$f_f = E_f\varepsilon_f \quad \text{if } \varepsilon_f \le \varepsilon_{fu} \tag{10}$$

$$f_f = 0 \quad \text{if } \varepsilon_f \le \varepsilon_{fu} \tag{11}$$

Where:
f_f = Tensile stress in FRP rebar
E_f = FRP modulus of elasticity
ϵ_f = Tensile strain in FRP rebar
ϵ_{fu} = Failure tensile strain for FRP rebar
F_{fu} = Failure tensile stress for FRP rebar

Moment-curvature relationship: Figure 2 shows H-RC rectangular beam section having steel and FRP reinforcing rebar at top and bottom, the process of analysis begins by supposing a little initial strain value for outer concrete level of compression zone (i.e., ϵ_c = 0.00001) with incremental strain 0.00001 upward till concrete crushing strain (ϵ_{cu} = 0.0038). For each value of assumed strain ϵ_c one loop carried out through repeated steps. Initially, the depth of neutral axis is assumed (x_c). Consequently, strains for the extreme fiber of concrete in tension zone and FRP-/steel-reinforcement rebar at top and bottom level is determined. The consistent assuming criterions comprised, the study plane before bending is continues plane after bending and perfectly bonding through surfaces of reinforcements and surrounding concrete. Next these strains values used to calculate the corresponding stresses for each material using their coincided stress-strain relationship presented in Fig. 1. Then, the relative forces are determined and the equilibrium condition of forces is satisfied. These steps are repeated using iterative method called bi-section method in which two values of the neutral axis depth (x_c) is assumed one for each sides of the correct value (i.e., $x_{c,\,top}$ = 0 at the top level and $x_{c,\,bottom}$ = h where h = overall section depth). Finally, the corrected value is utilized with accuracy of ξ = ±0.0001 for equilibrium forces condition.

The strain at each level in hybrid reinforced concrete section is linear proportion to its dimension from the neutral axis as shown in Fig. 2, the tensile strain in concrete at extreme fiber in tension zone described as follows:

$$\varepsilon_t = \frac{h\text{-}x_c}{x_c}\,\varepsilon_c \tag{12}$$

Since, a fully bonding is assumed between reinforcement rebar and surrounding concrete, thus, the strain initiated in tension and compression steel and FRP rebar stated in Eq. 13-16 as follows:

$$\varepsilon_f' = \frac{d_f'\text{-}x_c}{x_c}\,\varepsilon_c \tag{13}$$

$$\varepsilon_f = \frac{d_f\text{-}x_c}{x_c}\,\varepsilon_c \tag{14}$$

$$\varepsilon_s' = \frac{d_s' - x_c}{x_c}\,\varepsilon_c \quad (15)$$

$$\varepsilon_s = \frac{d_s - x_c}{x_c}\,\varepsilon_c \quad (16)$$

Where:

ϵ_f' and ϵ_f = The strain at top and bottom FRP reinforcing rebar

d_s' and d_s = The top and bottom FRP-reinforcing depth, respectively

ϵ_s' and ϵ_s' = The strain at top and bottom steel-reinforcing rebar

d_s' and d_s' = The top and bottom steel-reinforcing depth, respectively

To determine the resultant for the internal concrete compression forces at any loading stage, rational integration approach is used along the neutral axis depth with transformation the compression concrete stress (f_c) in term of x_c instead of ϵ_c as descried in Eq. 17-19:

$$F_c = b\int_0^{\varepsilon_{ca}} f_c(\varepsilon_c)\,d\varepsilon_c = b\int_0^{x_{ca}} f_c(x_c)\,\frac{\varepsilon_{co}}{x_{co}}\,dx \quad (17)$$

$$f_c(x_c) = f_c'\left(\frac{2x_c}{x_{co}} - \left(\frac{x_c}{x_{co}}\right)^2\right) \text{ if } x_c \le x_{co} \quad (18)$$

$$f_c(x_c) = f_c'\left(1 - 0.15\,\frac{(x_c - x_{co})}{(x_{cu} - x_{co})}\right) \text{ if } x_{co} < x_c \le x_{co} \quad (19)$$

Where:

F_c = Compression forces resultant of concrete

b = Beam width

ϵ_{ca} = Assumed concrete strain

x_c = Neutral axis depth at ϵ_{co}

x_c = Neutral axis depth at ϵ_c

$f_c(x_c)$ = Compressive stress function in terms of neutral axis depth

x_{cu} = Neutral axis depth at ϵ_{cu}

The tension forces resultant of concrete (T_c) is determined based on the internal tensile stress of concrete in tension zone with corresponding value of tensile strain (ϵ_t) and (ϵ_c) (Eq. 12). Simple triangle and trapezoidal relationships are used to evaluate internal forces as shown in Fig. 3, then concrete tension resultant is obtained at each stage of loading as descried in Eq. 20-23:

$$T_c = \frac{b}{2}\times x_t \times f_t(\varepsilon_t) \text{ if } 0 \le \varepsilon_t \le \varepsilon_0' \quad (20)$$

where $x_t = (h - x_c)$.

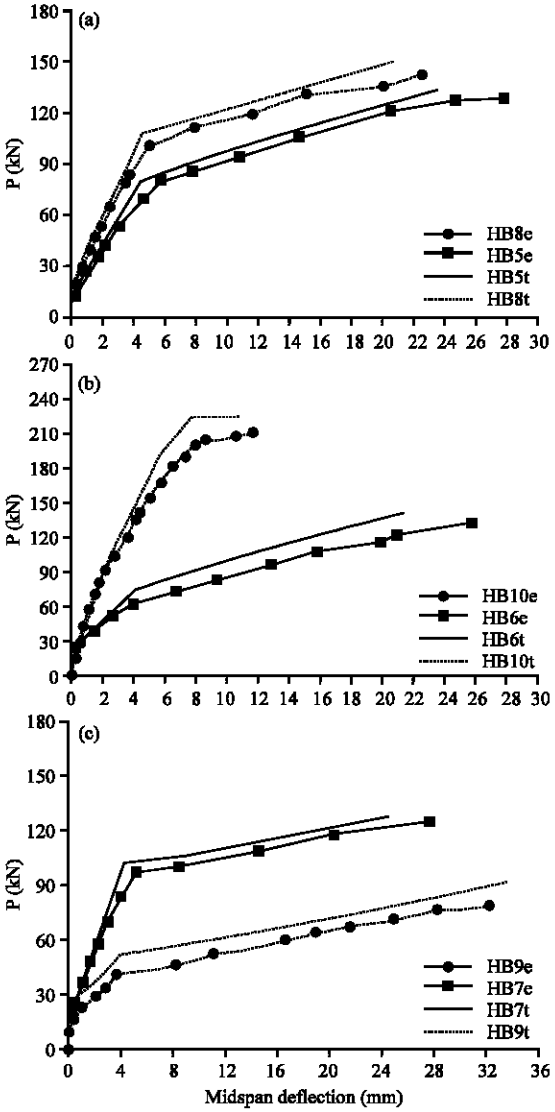

Fig. 3: a-c) Comparisons of load deflection curves of experimental tests (Qu *et al*., 2009) and prediction theoretical model (Qu *et al*., 2009)

$$T_c = T_{co} + \frac{b}{2}\times(x_t - x_{to})\times(0.8\,f_t' + f_t(\varepsilon_t)) \text{ if } \varepsilon_0' < \varepsilon_t \le 4\varepsilon_0' \quad (21)$$

where, $T_{co} = b/2\times x_{to}\times f_t'$, $x_{to} = x_t\times\epsilon_0'/\epsilon_t$.

$$T_c = T_{co} + T_{co4} + \frac{b}{2}\times(x_t - x_{to4})\times(0.45\,f_t' + f_t(\varepsilon_t)) \text{ if } 4\varepsilon_0' < \varepsilon_t \le F_t\,\varepsilon_0' \quad (22)$$

where, $T_{co4} = b/2\times(x_{to4} - x_{to})\times 1.25\,f_t'$, $x_{to4} = x_t\times 4\epsilon_0'/\epsilon_t$.

$$T_c = T_{co} + T_{co4} + T_{coFt} \text{ if } \varepsilon_t > F_t\,\varepsilon_0' \quad (23)$$

where, $T_{coFt} = b/2\times(x_{coFt} - x_{to4})\times 0.45\,f_t'$, $x_{toFt} = x_t\times F_t\,\epsilon_0'/\epsilon_t$.

The components of force for the FRP and steel rebar for the top and bottom of cross section are calculated according to the reinforcing as illustrated in Eq. 24-31:

$$T_s = A_s E_s \varepsilon_s \text{ if } 0 \le \varepsilon_s \le \varepsilon_y \quad (24)$$

$$T_s = A_s f_y \text{ if } \varepsilon_s > \varepsilon_y \quad (25)$$

$$C_s = A_s' E_s \varepsilon_s' \text{ if } 0 \le \varepsilon_s' \le \varepsilon_y \quad (26)$$

$$C_s = A_s' f_y \text{ if } \varepsilon_s' > \varepsilon_y \quad (27)$$

$$T_f = A_f E_f \varepsilon_f \text{ if } 0 \le \varepsilon_f \le \varepsilon_{fu} \quad (28)$$

$$T_f = 0 \text{ if } \varepsilon_f > \varepsilon_{fu} \quad (29)$$

$$C_f = A_f' E_f \varepsilon_s' \text{ if } 0 \le \varepsilon_s' \le \varepsilon_{fu} \quad (30)$$

$$C_f = 0 \text{ if } \varepsilon_s' > \varepsilon_{fu} \quad (31)$$

Where:

T_s = Tensile force of bottom steel rebar
A_s = Reinforcing area of bottom steel rebar
C_s = Compressive force of top steel rebar
A_s' = Reinforcing area of top steel rebar
T_f = Tensile force of bottom FRP rebar
A_f = Reinforcing area of bottom FRP rebar
C_f = Compressive force of top FRP rebar
A_f' = Reinforcement area of top FRP rebar
E_f = Elasticity modulus of FRP rebar (assuming same behaviour of FRP rebar in tension and compression)

Taking into account the equilibrium condition of forces, the forces resultant of hybrid reinforced cross section shown in Fig. 2 must be equated to required accuracy (i.e., $\xi = \pm 0.0001$) in the prediction theoretical model as given in Eq. 32:

$$F_c + C_s + C_f - T_s - T_f = \xi \quad (32)$$

Equation 32 represents the final repeating steps in iterative process (i.e., bi-section method) to find the corrected value of neutral axis depth x_c where the sufficient equilibrium accuracy is reached. From the strain distribution shown in Fig. 2b, the beam curvature Ø can be evaluated as described in Eq. 33:

$$\varnothing = \frac{\varepsilon_c}{x_c} \quad (33)$$

Since, all internal forces of hybrid cross section are established for assumed value of compression concrete strain at extreme top fiber (ϵ_c), then the corresponding stage of loading can be identified by calculating the applied moment M_{app} by taking a moment about any horizontally axis such as neutral axis as specified in Eq. 34:

$$M_{app} = F_c (x_{cen}) + C_s(x_c - d_s') + C_f(x_c - d_f') + T_s(d_s - x_c) + T_f(d_f - x_c) \quad (34)$$

Where:

M_{app} = Applied moment of H-RC section
x_{cen} = Distance between the axis of concrete compressive resultant and neutral axis

Mid-span deflections: Since, the moment-curvature relationship of H-RC beam has been provided, the flexural rigidity of the beam El_{eff} can be developed at each stage of loading as in Eq. 35:

$$El_{eff} = \frac{M}{\varnothing} \quad (35)$$

The central span deflection (Δ) of H-RC members can be calculated at each loading stage using the formula of elastic deflection with specific loading system, instance, the mid-span deflection of simple supporting members having two-point loading (P/2) can be obtained using Eq. 36:

$$\Delta = \frac{23}{1.296} \frac{PL^3}{El_{eff}} \quad (36)$$

Where:

Δ = Central span deflection
P = Applied load
L = Member span

For simply supported members with central point load (P), the mid-span deflection can be determined as illustrated in Eq. 37:

$$\Delta = \frac{1}{48} \frac{PL^3}{El_{eff}} \quad (37)$$

RESULTS AND DISCUSSION

Verification of theoretical predicted model with test results: Verification of the theoretical model of hybridization FRP/steel reinforcing concrete member is carried out through a comparison of the prediction model results and the tested results for the same cross sectional

shape (i.e., rectangular cross section) with various conditions of geometrical, mechanical properties and loading pattern that is to examine the suitability of adopted model to analyze H-RC members. Table 1 shows the geometry and mechanical details of (19) H-RC members. Mainly, comparisons are introduced in terms of the bending moment capacity ratio and load deflection responses that is to investigate the coincidence degree of the prediction technique in applications.

Flexural capacity ratio: Since, all tested beams were designed to fail in flexural failure as described in literature, the flexural capacity of each beam is compared between the prediction theoretical model and tested beams as illustrated in Table 2 where $M_{u, th}$ is the ultimate moment of theoretical model and $M_{u, exp}$ is the ultimate moment of experiment. The statistic coefficients mean, standard deviation and variation factor of the flexural capacities ($M_{u, th}/M_{u, exp}$) are 1.01, 11.88 and 1.41%, respectively and the variation of ratio ($M_{u, th}/M_{u, exp}$) in range of 0.79-1.12 reasonably well except HB10. As seen, a good agreement is achieved through comparison results, so, the theoretical model can be used in analysis of hybrid reinforcement concrete members.

Load-deflection response: The load-deflection relationship of H-RC member reflects the structural behaviour of material combination, concrete, steel and FRP reinforcement. Figure 3 presents the load deflection curve obtained using adopted technique in comparison with the results of HB5-HB10 which are tested by Qu *et al.* (2009). These tested results represent a good sample to proof the validity of prediction theoretical model because it contains a wide range values of the

Table 1: Geometric and mechanical details of tested HRC-beams in literature

Beam No.	b×h×L (mm)	$n_s b_{ds}$ (mm)	A_s (mm^2)	b_{df} (mm^2)	A_f (mm^2)	A_s' (mm)	E_s (GPa)	F_y (MPa)	E_f (GPa)	f_{fu} (MPa)	f_c' (MPa)	f_t' (MPa)	Load system
HB1 (Aiello and Ombres 2000)	b=150	2⌀8	100.5	27.5	88.3	100.50	200	465	49.0	1674	36.56	4.03	4-point
HB2 (Aiello and Ombres 2000)	h=20	2⌀8	100.5	210	157.0	100.50	200	465	50.1	1366	36.56	4.03	4-point
HB3 (Aiello and Ombres 2000)	L=2700	2⌀8	100.5	310	235.5	100.50	200	465	50.1	1366	36.56	4.03	4-point
HB4 (Aiello and Ombres 2000)		2⌀8	100.5	27.5	88.3	100.50	200	465	49.0	1674	36.56	4.03	4-point
HB5 (Qu *et al.*, 2009)		2⌀12	226.1	212.7	253.2	-	200	363	45.0	782	26.48	10.31	4-point
HB6 (Qu *et al.*, 2009)	b=180	1⌀16	201.0	215.9	396.9	-	200	336	41.0	755	26.48	10.31	4-point
HB7 (Qu *et al.*, 2009)	h=250	2⌀16	401.9	29.5	141.7	-	200	336	37.7	778	27.52	10.58	4-point
HB8 (Qu *et al.*, 2009)	L=2100	2⌀16	401.9	212.7	253.2	-	200	336	45.0	782	27.52	10.58	4-point
HB9 (Qu *et al.*, 2009)		1⌀12	113.0	29.5	141.7	-	200	363	37.7	778	32.52	11.82	4-point
HB10 (Qu *et al.*, 2009)		6⌀16	1205.8	215.9	396.9	-	200	336	41.0	755	32.52	11.82	4-point
HB11 (Lau and Pam, 2010)	b=280	2⌀25	981.7	119	283.5	56.55	181	336	39.5	588	41.30	13.21	3-point
HB12 (Lau and Pam, 2010)	h=380	2⌀20	628.3	225	981.7	56.55	190	597	38.0	582	39.80	12.84	3-point
HB13 (Lau and Pam, 2010)	L=4200	2⌀25	981.7	219	567.1	56.55	196	550	39.5	588	44.60	12.99	3-point
HB14		1⌀10	78.5	212	226.2	100.50	200	520	50.0	1000	40.00	11.70	4-point
HB15	b=230	2⌀10	157.1	212	226.2	100.50	200	520	50.0	1000	40.00	11.70	4-point
HB16	h=300	2⌀12	226.2	212	226.2	100.50	200	520	50.0	1000	40.00	11.70	4-point
HB17	L=3700	2⌀10	157.1	216	402.1	100.50	200	520	50.0	1000	40.00	11.70	4-point
HB18		2⌀12	226.2	216	402.1	100.50	200	520	50.0	1000	40.00	11.70	4-point
HB19		2⌀16	402.1	216	402.1	100.50	200	520	50.0	1000	40.00	11.70	4-point

Table 2: Comparison ultimate bending strength of hybridization reinforcing concrete members

Beam No.	A_f/A_s	$M_{u, exp}$ (kN.m)	$M_{u, th}$ (k Nm)	$(M_{u, th}/M_{u, exp})$
HB1 (Aiello and Ombres 2000)	0.88	25.14	19.79	0.79
HB2 (Aiello and Ombres 2000)	1.56	28.41	25.21	0.89
HB3 (Aiello and Ombres 2000)	2.34	35.55	29.62	0.83
HB4 (Aiello and Ombres 2000)	0.88	25.14	20.94	0.83
HB5 (Qu *et al.*, 2009)	1.12	38.28	39.68	1.04
HB6 (Qu *et al.*, 2009)	1.98	39.66	42.76	1.08
HB7 (Qu *et al.*, 2009)	0.35	36.36	38.95	1.07
HB8 (Qu *et al.*, 2009)	0.63	42.57	44.09	1.04
HB9 (Qu *et al.*, 2009)	1.25	23.55	29.86	1.27
HB10 (Qu *et al.*, 2009)	0.33	63.30	70.83	1.12
HB11 (Lau and Pam, 2010)	0.29	147.00	157.49	1.07
HB12 (Lau and Pam, 2010)	1.56	261.00	226.6	0.87
HB13 (Lau and Pam, 2010)	0.58	229.00	238.75	1.04
HB14	2.88	47.62	51.86	1.09
HB15	1.44	53.55	57.06	1.07
HB16	1.00	58.94	61.73	1.05
HB17	2.56	68.30	71.03	1.04
HB18	1.78	64.71	68.23	1.05
HB19	1.00	83.53	86.21	1.03
The average	1.01			

hybrid reinforcement ratio between reinforcing area of FRP (A_f) and reinforcing area of steel (A_s) under same circumstance geometrical and mechanical conditions. Although, the samples chosen in Fig. 3a-c have considerable difference in hybrid reinforcement ratio (A_f/A_s), the comparison of corresponding curves of experimental results and theoretical model are convergent with acceptable degree. Thus, the prediction theoretical model can be used in applications and parametric studies to distinguish the effectiveness of mechanical and geometrical properties of hybrid reinforcements members.

In general view, the load deflection curve of H-RC section contains three stages, namely uncrack section stage, cracked section stage and yielding section stage as shown in Fig. 3. Each phase affected by geometrical and mechanical properties of collective materials and relative relation among them. Initially, first stage is a linear part terminated when the members starting cracked and secondly stage part had a reduction in grade than the first line owing to decrease in beam stiffness after cracking. Finally, yield section segment started when steel reinforcement is yielded which caused higher reduction in beam stiffness and FRP reinforcement plays the role in resisting the load in this stage.

Stiffness tension effects: Including the tension stiffness in theoretical predictions increased the accuracy of theoretical results especially up to the stage of serves loading (i.e., about 65% of ultimate load), since, the effects of tension stiffness is decreased with increased loading (Qu *et al*., 2009). The predicted theoretical model is employed to study the effects of tension stiffness in structural performance H-RC members on the load deflection response as presented in Fig. 4. The geometrical and mechanical properties of case study used in Fig. 4 are simply supported beam with four-point loading, the dimensions L = 4500 mm, b = 250, h = 400 mm, $d_s = d_f = 357$ mm and the mechanical properties of concrete $f_c' = 28$ MPa, $f_t' = 3.28$ MPa steel rebar $f_y = 420$ MPa, $E_s = 200$ GPa and GFRP rebar $f_{fu} = 1000$ MPa, $E_f = 40$ GPa. In design calculation, the tension stiffness in concrete is neglected for simplicity in this case the first linear segment in load-deflection curve is omitted and the load-deflection curve become two linear parts divided by yielding point as shown in Fig. 4. Also, a small reduction in stiffness beam, yield strength is appeared while approximately the same ultimate strength value as seen. In addition, the tension stiffness is affected by the area of steel/FRP reinforcement with same (A_f/A_s), so that as the area of reinforcement increased the effects of tension

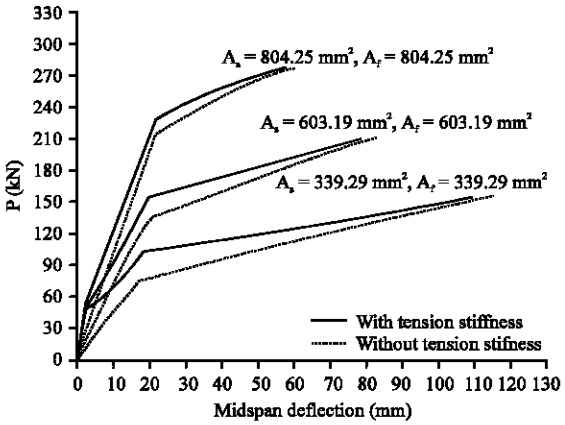

Fig. 4: Tension stiffness effects on load deflection curve of H-RC member

stiffness is decreased due to increasing in flexural capacity which is diminished the effects of tension stiffness.

Frp reinforcement type effects: The type of FRP reinforcement in H-RC members effects shown in Fig. 5. The same dimensions and material properties of case study are used with the same area of reinforcements $A_f = 603.19$ mm², $A_s = 603.19$ mm² and AFRP rebar $f_{fu} = 1300$ MPa, $E_f = 60$ GPa and CFRP rebar $f_{fu} = 1500$ MPa, $E_f = 120$ GPa. The effects of FRP reinforcement is null in the first stage of load-deflection curve because of low loading phase and uncrack concrete section while the effects are slightly improvements in the second stage owing to higher value of elastic modulus of steel reinforcement compared with those elastic moduli of FRP reinforcement and clearly effects of FRP reinforcements appeared on the third stage of load-deflection curve due to yielding of steel rebar and the FRP rebar become the core of reinforcements resistance at this stage.

Reinforcements ratio of H-RC section: The reinforcement ratio of H-RC section effectively affects the structural behaviour of members, since, the value of reinforcement ratio indicate the type of expected failure modes. Also, the structural behaviour of H-RC section with any (A_f/A_s) ratio is similar of S-RC members with the same equivalent steel reinforcement ratio ($\rho_{eq,s}$), since, they coincided up to the yield point stage of loading which is an important loading stage for design purpose as shown in Fig. 6. The difference between them occurred in the third stage of load-deflection curve due to present FRP-reinforcement in H-RC section which can be considered as the reserve strength. Thus, it is useful to specify the hybrid

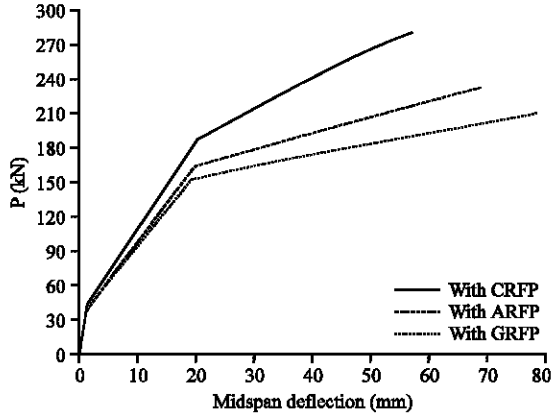

Fig. 5: Effects of FRP types on load deflection curve of H-RC member

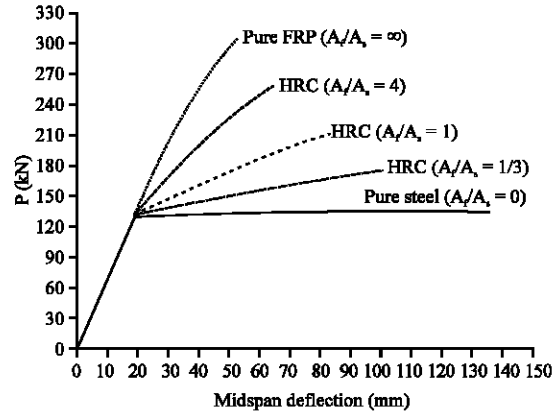

Fig. 6: Load-deflection curve of H-RC section with same equivalent reinforcement ratio ($\rho_{eq,s}$ = 0.811%) and different (A_f/A_s) ratio

reinforcement ratio in H-RC section in terms of the equivalent steel reinforcement ratio ($\rho_{eq,s}$) rather than the equivalent FRP reinforcement ratio ($\rho_{eq,s}$), since, the latter linear up to failure (i.e., without yield point). The equivalent steel or FRP reinforcement ratio of H-RC section are defined as following:

$$\rho_{eq,s} = \rho_s + \rho_f \frac{E_f}{E_s} \quad (38)$$

$$\rho_s = \frac{A_s}{b\, d_s} \quad (39)$$

$$\rho_f = \frac{A_f}{b\, d_f} \quad (40)$$

Where:

ρ_s = steel reinforcement ratio

ρ_f = FRP reinforcement ratio

$$\rho_{eq,f} = \rho_s \frac{E_s}{E_f} + \rho_f \quad (41)$$

For clarification the effects reinforcements ratio on structural behaviour of H-RC members, the tension stiffness is neglected. Figure 6 presents the load deflection curves of case study of H-RC section with different values of (A_f/A_s) ratio, pure FRP-and pure steel- reinforcement sections are included with the same equivalent steel ratio (i.e., $\rho_{eq,s}$ = 0.811%) for all cases as details shown in Table 3.

It can be observe that the difference in behaviour among all cases under consideration in Fig. 6 commenced at the point of steel yielding. Although, all cases of H-RC beam have the same $\rho_{eq,s}$ (= 0.811%) but the ultimate strength is increased as the (A_f/A_s) ratio increased owing to increase in the amount area of FRP-reinforcement.

Failure modes of hybrid-RC section: The prediction theoretical model is employed to indicate the failure mode of H-RC members. The failure can be happened in H-RC section when one or more of material components fail induvial or simultaneously. The reinforcement ratio of H-RC section effectively affected the governing type of failure mode which can be distinguished according to limitations of reinforcement ratio specified in Eq. 45. When concrete crushing with steel reinforcement yielding simultaneously at which FRP reinforcement not ruptured yet in this case the balanced steel reinforcement ratio ($\rho_{s,b}$) can be calculated using consistent assumptions for equilibrium and compatibility relationships as follows:

$$\rho_{s,b} = 0.85\, \beta_1 \frac{f_c'}{f_y} \frac{E_s\, \varepsilon_{cu}}{f_y + E_s\, \varepsilon_{cu}} \quad (45)$$

Where, β_1 = 0.85-0.05 f_c'-28/7 when steel reinforcement yielding, then concrete crushing with FRP reinforcement ruptured simultaneously in such case the balanced FRP reinforcement ratio ($\rho_{f,b}$) can be obtained as:

$$\rho_{s,b} = 0.85\, \beta_1 \frac{f_c'}{Ff_{fu}} \frac{E_s\, \varepsilon_{cu}}{Ff_{fu} + E_s\, \varepsilon_{cu}} \quad (46)$$

In addition, a critical condition (i.e., "Not balanced" and it is occurred in tension zone) can be utilized when steel reinforcement yielding with FRP reinforcement ruptured simultaneously at which concrete crushing not yet occurred the critical steel-FRP reinforcement ratio ($\rho_{sf,c}$) can be obtained as:

Table 3: Reinforcements details of HRC-section with same value of equivalent reinforcement ratio ($\rho_{eq,s}$)

Case No.	A_s (mm^2)	ρ_s (%)	A_f (mm^2)	ρ_f (%)	$\rho_{eq,s}$ (%)	$A_{eq,s}$ (mm^2)	A_f/A_s
Pure-steel	723.83	0.811	0	0	0.811	723.83	0
HRC	678.58	0.760	226.250	0.254	0.811	723.83	1/3
HRC	603.19	0.676	603.190	0. 676	0.811	723.83	1
HRC	402.12	0.451	1608.550	1.8020	0.811	723.83	4
Pure-FRP	0.00	0.000	3619.150	4.0550	0.811	723.83	8

$$\rho_{sf,c} = \frac{f_y A_s + F_{fu} A_f}{f_{fu} b d_f} = \rho_s \frac{f_y}{f_{fu}} + \rho_f \quad (47)$$

According to the first material component failure and limitations of reinforcements ratio specified in Eq. (45-47) the failure modes of H-RC members can be illustrated as following.

Concrete crushing failure mode: This undesirable failure occurred if the equivalent steel reinforcement ratio ($\rho_{eq,s}$) is greater than the balanced steel reinforcement ratio ($\rho_{s,b}$) (i.e., over reinforced section) in which concrete crushing while steel-and FRP-reinforcements not yielding not ruptured yet, respectively.

FRP rupturing failure mode: This inadmissible failure mode occurred when ($\rho_{eq,s}$) ratio is less than ($\rho_{f,b}$) or ($\rho_{sf,c}$) ratio is less than ($\rho_{f,b}$).

Steel yielding failure mode: This is ductile and desirable failure mode, since, yielding of steel causes extensive previous warning. It is occurred when ($\rho_{eq,s}$) ratio is less than ($\rho_{s,b}$) (i.e., under reinforced section) and to control steel reinforcing yield followed by concrete crushing rather than FRP rebar ruptured, the value of ($\rho_{sf,c}$) ratio must be greater than ($\rho_{f,b}$).

Flexural design guidance of H-RC section singly reinforced: To mitigate the variation of practical strength of S-RC section and to ensure ductile failure mode ACI 318M-14 adopted approach of tension controlled section, so that, the nominal flexural strength determined when the tensile strain of outer steel layer is equal or more than (ϵ_s = 0.005) at which the concrete crushing is occurred simultaneously (ACI., 2006). Using tension controlled section in H-RC section, the upper limit of ($\rho_{eq,s}$) ratio is the maximum equivalent steel reinforcement ratio ($\rho_{s,max}$) which is determined in terms of ($\rho_{s,b}$) as:

$$\rho_{eq,s} = \rho_s + \rho_f \frac{E_f}{E_s} \leq \rho_{s,max} \quad (48)$$

$$\rho_{s,max} = \rho_{s,b} \frac{E_s \varepsilon_{cu} + f_y}{E_s \varepsilon_{cu} + 0.005 E_s} \quad (49)$$

In other hand, the same adopted approach of ACI 440.1R-06 for FRP-RC section (ACI., 2006) is used to ensure concrete crushing prior FRP-rupturing failure mode. Thus, the maximum equivalent FRP reinforcement ratio ($\rho_{f,b}$) which the upper limit of ($\rho_{eq,f}$) ratio is obtained regarding ($\rho_{f,b}$) as follows:

$$\rho_{sf,f} \geq \rho_{f,max} \quad (50)$$

$$\rho_{f,max} = 1.4\, \rho_{f,b} \quad (51)$$

Also to ensure steel yielding occurred before FRP-rupturing failure mode, the condition of steel yielding failure mode illustrated as follows:

$$\rho_{sf,c} \geq \rho_{f,max} \quad (52)$$

Basis on the concept of ACI 440-06 (i.e., ϕ Mn = Mcr where Mcr is the moment of cracking section) to specify the formula of minimum equivalent steel reinforcement ratio ($\rho_{s,min}$) for H-RC members as follows [12]:

$$\rho_{s,min} = \frac{0.25\sqrt{f'_c}}{f_y} \geq \frac{1.4}{f_y} \quad (53)$$

Ductility index of H-RC member: The definition of ductility can be summarized as the ability of structure to withstand the applied loading up to the ultimate load with large deformation before collapse. In ordinary S-RC structure, ductility index is recognized by a ratio of ultimate to the first steel-reinforcement yield deformations. However, Rashid *et al.* (2005) concluded that the traditional definition of ductility index in terms of deformability found to be inadequate for structure without yield point such as AFRP-RC beams. In energy basis, the ductility is identified as the ability of structure to absorbing the energy up to collapse. Tan (1997) suggested the ductility index as ratio between the total energy determined as area below the load-deflection curve and total elastic energy of corresponding case. Aiello and Ombres (2002) predicted (df) parameter which is represented as a ratio of area below the moment-curvature curve to that area determined up to

detecting curvature value. Qu *et al.* (2009) concluded that the ductility HRC members varied with (A_f/A_s) ratio and modulus of elasticity for FRP and steel reinforcements. Pang *et al.* (2015) proposed a definition of ductility index (μh) with energy and deformability basis for H-RC members as follows (Kara *et al.*, 2015):

$$\mu_h = \psi \frac{D_{uh}}{D_{uy}} \geq (\mu_D) \quad (54)$$

$$\psi = \frac{U_H}{U_s} \leq 1.0 \quad (55)$$

Where:

D_{uh} = Curvature, rotations and displacement at ultimate stage of loading

D_{uy} = Curvature, rotations and displacement at first steel yielding

H_h = Area below moment-curvature curve of H-RC member

U_s = Area below moment-curvature curve of equivalent S-RC member

ψ = Factor of ductility reduction

μ_D = Traditional definition of SRC beams (Kara *et al.*, 2015)

By reviewing the verification test results of last proposed ductility index, it is found that the factor of ductility (ψ) values gives a significant meaning for beam's ductility rather than the proposed ductility index (μh), since, the factor ψ is scaled the ductility index of H-RC member with respect to reference point (i.e., ψ = 1.0) represented by S-RC member reinforced with equivalent steel reinforcement ratio ($\rho_{eq,s}$). Figure 7 shows the modified ductility index (ψ) verses the (A_f/A_s) ratio for the case study under consideration with range values of ($\rho_{eq,s}$) ratio from ($\rho_{eq,s} = \rho_{s,min} = 0.33\%$) to ($\rho_{eq,s} = \rho_{s,b} = 3.01\%$). It seem that the as the (A_f/A_s) increased the ductility of H-RC members decreased as expected, since, the amount of steel reinforcement decreased. In addition, the range of variation of ductility index (ψ) is receded as the equivalent steel reinforcement ratio ($\rho_{eq,s}$) is increased because of increasing the amount of reinforcing steel rebar which is eliminated the effect of FRP reinforcement in other words as the ($\rho_{eq,s}$) ratio increased the ratio between load causing yielding steel to ultimate load (P_f/P_s) is increased.

Effective range of (A_f/A_s) ratio of hrc member: In HRC members, the steel reinforcement is introduced to improve ductility and stiffness while the FRP reinforcements essentially to increase the ultimate strength and to migrate corrosion of steel reinforcement. These two criteria are acted in opposite direction, thus by intersecting these two criteria with various amount of equivalent steel reinforcement ratio, the critical behaviour of H-RC beams can be achieved. The theoretical prediction model is used to investigate the effective range of (A_f/A_s) ratio in H-RC beams for the case study. Figure 8 represents the variation of ductility index (ψ) and normalized ultimate strength index ($X = P_{u,h}/P_{u,f}$) verse the (A_f/A_s) ratio of case study considered in this study. where, $P_{u,h}$ = Ultimate strength of H-RC members and $P_{u,f}$ = Ultimate strength of FRP-RC members reinforced by FRP reinforcement with the same equivalent steel reinforcement ratio ($\rho_{wq,s}$). Three values of ($\rho_{eq,s}$) ratio were used, namely ($\rho_{eq,s} = \rho_{s,min} = 0.33\%$, $\rho_{eq,s} = \rho_{s,max} = 1.98\%$ and $\rho_{eq,s} = \rho_{eq,s} = 3.01\%$) to indicate limits of the critical range of ($\rho_{eq,s}$) ratio that meets the ductility index (ψ) and ultimate strength index (ψ) at same level as shown in Fig. 8. It shows that the critical range of the (A_f/A_s) ratio for the case study is limited between (A_f/A_s = 1.40 for $\rho_{eq,s} = \rho_{s,min} = 0.33\%$) and ($A_f/A_s$ = 0.59 for $\rho_{eq,s} = \rho_{s,b} = 3.01\%$).

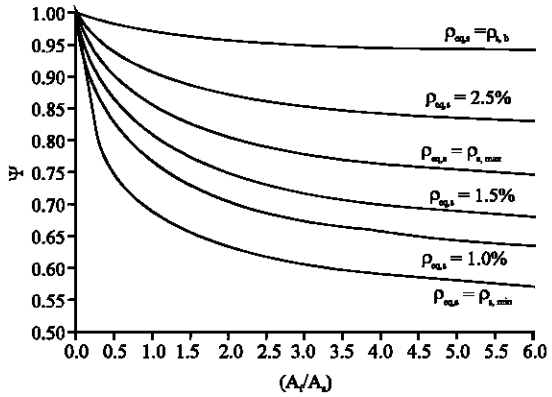

Fig. 7: Variation of ductility index (ψ) of H-RC case study member against (A_f/A_s) ratio

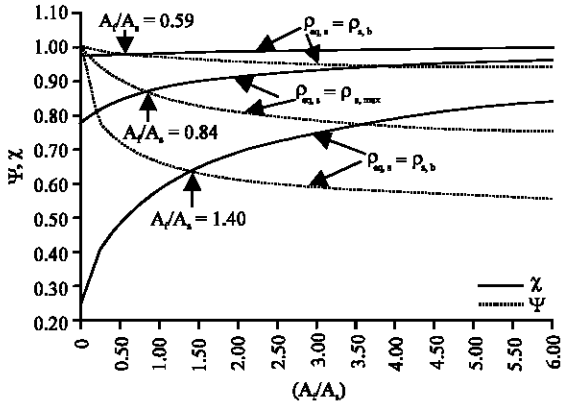

Fig. 8: Effective limits range of (A_f/A_s) ratio for HRC members

CONCLUSION

Theoretical model of analysis hybrid reinforced FRP and steel concrete member is presented using principle of strain compatibility and forces equilibrium, the moment-curvature relation, deflection and ultimate moment strength are established. A good a agreements have been shown between theoretical prediction results and experimental results of other researcher. The adopted stress-strain relationships for concrete in compressive and tensile zones in the theoretical model are suitable with acceptable degree of coinciding in load-deflection response.

Tension stiffness of concrete in H-RC section has significant effects in the first part of load-deflection curve and this effect is lessened in second stage of curve while it is diminished in the third stage and ultimate strength of H-RC members.

The effectiveness type of FRP reinforcements in H-RC member is augmented as it's modulus of elasticity increased, since, the FRP reinforcements plays a role in the third stage of load deflection curve of HRC member after yielding of steel is occurred.

The principle of converting the FRP reinforcement in HRC section into equivalent steel reinforcement can be adopted to apply provisions of ACI-318M-14 in designing approach with modifying formula, since, the recommended failure in HRC is ductile failure mode initiated by steel yield then concrete crushing while FRP rebar not yet ruptured. The equivalent steel reinforcement ratio is affected by elasticity modulus of FRP rebar.

The ductility index of H-RC beam represented by the ratio of total absorption energy of H-RC beam to total absorption energy of S-RC beam reinforced with equivalent steel ratio. While the ultimate strength index of H-RC beam identified as the ratio between the ultimate bending strength of H-RC member to that for FRP-RC beam reinforced by FRP reinforcement with the same equivalent steel reinforcement ratio. The variation of these indices are opposed as the equivalent reinforced ratio (A_f/A_s) is increased due to increase of FRP reinforcing area with respect to decrease of steel reinforcement.

Critical range of hybrid reinforcement (A_f/A_s) ratio are specified that meets the ductility index (ψ) and normalized ultimate strength index (X) at the same level.

REFERENCES

ACI, 318-05, 2005. Building Code Requirements for Structural Concrete and Commentary. ACI Committee 318, American Concrete Institute, Farming Hills, MI, USA., pp: 430.

ACI., 2006. 440.1R-06: Guide for the Design and Construction of Structural Concrete Reinforced with FRP Bars. American Concrete Institute, Michigan, USA., ISBN:9780870312106, Pages: 44.

Aiello, M.A. and L. Ombres, 2000. Load-deflection analysis of FRP reinforced concrete flexural members. J. Compos. Constr., 4: 164-171.

Bischoff, P.H. and R. Paixao, 2004. Tension stiffening and cracking of concrete reinforced with Glass Fiber Reinforced Polymer (GFRP) bars. Can. J. Civil Eng., 31: 579-588.

Hawileh, R.A., 2015. Finite element modeling of reinforced concrete beams with a hybrid combination of steel and ARAMID reinforcement. Mater. Des., 65: 831-839.

Kara, I.F., A.F. Ashour and M.A. Koroglu, 2015. Flexural behavior of hybrid FRP-steel reinforced concrete beams. Compos. Struct., 129: 111-121.

Lau, D. and H.J. Pam, 2010. Experimental study of hybrid FRP reinforced concrete beams. Eng. Struct., 32: 3857-3865.

Leung, H.Y. and R.V. Balendran, 2003. Flexural behaviour of concrete beams internally reinforced with GFRP rods and steel rebars. Structur. Surv., 21: 146-157.

Nayal, R. and H.A. Rasheed, 2006. Tension stiffening model for concrete beams reinforced with steel and FRP bars. J. Mater. Civil Eng., 18: 831-841.

Pang, L., W. Qu, P. Zhu and J. Xu, 2015. Design propositions for hybrid FRP-steel reinforced concrete beams. J. Compos. Constr., 20: 04015086-04015086.

Qu, W., X. Zhang and H. Huang, 2009. Flexural behavior of concrete beams reinforced with hybrid (GFRP and steel) bars. J. Compos. Constr., 13: 350-359.

Rashid, M.A., M.A. Mansor and P. Paramasivam, 2005. Behaviour of aramid fiber reinforced polymer reinforced high strength concrete beams under bending. J. Compos. Construct., 9: 117-127.

Tan, K.H., 1997. Behaviour of hybrid FRP-steel reinforced concrete beams. Proceedings of the 3rd International Symposium on Non-Metallic (FRP) Reinforcement for Concrete Structures (FRPRCS'97) Vol. 2, October 14-16, 1997, Japan Concrete Institute (JCI), Tokyo, Hokkaido, Japan, ISBN:4931451004, pp: 487-494.